Molecular Dynamics Study of Solvent Transport in Nanoscale Osmosis

doi: 10.1143/JPSJ.77.064605

Molecular Dynamics Study of Solvent Transport in Nanoscale Osmosis

Tomoaki ITANO, Takeshi AKINAGA, Masako SUGIHARA-SEKI

Department of Pure and Applied Physics, Faculty of Engineering Science, Kansai University
Suita, Osaka, 564-8680, Japan

An ideal of osmotic equilibrium between an ideal solution and pure solvent separated by a semi-permeable membrane is studied numerically using the method of molecular dynamics. The osmotic flow is observed as the inflow of the solvent across the membrane from the dilute to the concentrated side. The validity of van't Hoff's law for osmotic pressure is confirmed over a wide range of concentrations. It is found that the law is established by a balance between non-uniform partial pressures of solute and solvent. Furthermore, the present model permits an understanding of the mechanism of the osmotic flow in the relaxation process as the liquids evolve from the initial state to the equilibrium state. We focus in particular on the interaction between solute and solvent.

KEYWORDS: osmosis, ideal solution, molecular liquids, membrane processes, relaxation process, nanofluidics, molecular dynamics

1. Introduction

Osmosis is a fundamental physical process encountered in many fields of study, including biology, chemistry and medicine, as well as physics. It is well known that the permeability of most of biological and artificial membranes to water is greater than their permeability to many dissolved solutes. Suppose that a dilute solution is separated from a more concentrated solution by such a semi-permeable membrane, with both solutions subject to an external pressure. A movement of solvent through the membrane from the dilute to the concentrated side, the so-called osmotic flow, will be driven spontaneously. However, the consequent difference in the hydrostatic pressures either side of the membrane acts to oppose this flow. This difference in the magnitudes of the pressures is the original definition of osmotic pressure. The static equilibrium state that is finally reached subject to the osmotic pressure is termed "osmotic equilibrium". As an example of the application of osmotic pressure, the physiological saline used to maintain living tissue is normally designed to be isotonic to body fluids, since otherwise the osmotic pressure acting on membranes can give rise to the rupture of blood vessels and tissues.

The formulation of osmotic equilibrium was first established by J. van't Hoff[1)] in 1887. Since then, the formulation of the thermodynamics used to determine osmotic pressure has been refined by many studies.[2)] The present study considers osmotic flow and osmotic equilibrium from a kinetic molecular theory perspective. Murad & Powles[3)] and Raghunathan &

Aluru (2006)[4] recently adopted such a perspective, using specialized models for specific solvent/solute pairs to model osmotic equilibrium. In contrast, in the present study, it is intended to adopt a simple model to educe the underlying mechanisms of osmotic equilibrium that are valid for a range of solvent/solute combinations, and also to examine the relaxation process that occurs in order for the equilibrium to be established. It is of interest to determine whether consideration of molecular motions, even under the simplest conditions, can lead to the same results as those obtained by van't Hoff. Furthermore, such an approach may provide a more vivid picture of molecular motions, both of the equilibrium state, and also in the relaxation process as the solution evolves towards this equilibrium state.

Thus, in the present study, first we employ a molecular dynamics simulation to numerically reproduce a real liquid. Next, upon introducing an ideal solution of the liquid, and applying this solution to a reservoir separated into two regions by an idealized semi-permeable membrane, we then use this model to realize an ideal of osmotic equilibrium. We examine the validity of van't Hoff's law for this system. Finally, investigating the non-uniformity of the partial pressure of solute and solvent, we will discuss the mechanism of the osmotic flow, focusing in particular on the interaction between solute and solvent.

2. Formulation

We employ molecular dynamics (MD) to investigate a conventional micro-canonical ensemble of N mono-atomic molecules, enclosed in a reservoir with a volume V. The molecules interact through a two-body potential of Lennard-Jones type, $\phi(r) = 4\varepsilon\{(\frac{r}{\sigma})^{-12} - (\frac{r}{\sigma})^{-6}\}$, with cutoff radius $r_{\rm cut} = 2.5\sigma$. With this configuration, our task is to integrate the equations of motion according to classical mechanics, $m\frac{{\rm d}^2\boldsymbol{x}_i}{{\rm d}t^2} = \sum_{j(\neq i)} \boldsymbol{f}(\boldsymbol{x}_j - \boldsymbol{x}_i)$, where m denotes the mass of both the solvent and solute molecules, $\boldsymbol{x}_i$ is the position of the i-th molecule at time t and $\boldsymbol{f}(\boldsymbol{r}) = -\frac{\partial\phi}{\partial r}\frac{\boldsymbol{r}}{r}$. We adopt the velocity Verlet method with $\Delta t = 5 \times 10^{-4}$ as the time-development scheme, applied together with the neighbour list method[5] (see[6] for more details).

Henceforth, all the quantities will be measured in the following dimensionless units: The lengths are specified in units of σ, the energies in units of ε, and masses in units of m. For argon, $\sigma = 3.405$ Å, $\varepsilon/k_B = 119.8$ °K and $mN_A = 39.95$ g, and the time unit is therefore $\sqrt{\sigma^2 m/\varepsilon} = 2.16$ps. Throughout the present study, the density of the molecules is kept constant at 0.807, which is comparable to that of liquid argon. The thermodynamical quantities presented here are the long-time averages, denoted by $\langle\cdot\rangle = \frac{1}{T}\int_0^T {\rm d}t(\cdot)$, unless noted otherwise.

3. Results

3.1 Liquid in a cubic reservoir

First, we show that our Lennard-Jones model molecular system can be considered to be in the liquid phase for the selected parameter values, and not in gas or solid phases. With this

Table I. Values of parameters and thermodynamical quantities for the reservoirs of the present study and the Lennard-Jones molecular systems they contain. The density is fixed at $\rho = 0.807$, while the temperature is kept within a small range, $k_B\theta = 0.833 \sim 0.838$, by manipulating the initial conditions of the simulations. Periodic boundary conditions are denoted by 'P', while the reflective boundary conditions are denoted by 'R'.

	N	L_x	L_y	L_z	B.C.	T	$k_B\theta$	p	$-[\mathcal{P}]_{xx}$	$-[\mathcal{P}]_{yy}$	$-[\mathcal{P}]_{zz}$
pc1	512	8.59	8.59	8.59	P	200000	0.8376	0.9790	n/a	n/a	n/a
pc2	4096	17.18	17.18	17.18	P	200000	0.8380	0.9799	n/a	n/a	n/a
rc1	512	8.59	8.59	8.59	R	200000	0.8338	0.9856	0.9865	0.9866	0.9865
rc2	4096	17.18	17.18	17.18	R	200000	0.8355	0.9881	0.9884	0.9885	0.9885
rr1	2×512	2×8.59	8.59	8.59	R	200000	0.8368	0.9873	0.9346	1.0155	1.0153
rr2	2×4096	2×17.18	17.18	17.18	R	70000	0.8383	0.9931	0.9660	1.0074	1.0072

aim, we will estimate the pressure of an assembly of real argon atoms equivalent to our system, and then show that this assembly is in the liquid phase. The pressure can be calculated by applying Clausius' virial theorem to our system: $p_{\rm ar} = \frac{N}{V}k_B\theta + \frac{1}{6V}\sum_{i\neq j}\langle(\boldsymbol{x}_i - \boldsymbol{x}_j)\cdot\boldsymbol{f}(\boldsymbol{x}_j - \boldsymbol{x}_i)\rangle$, where θ is the temperature, which is related to the total kinetic energy of the molecules by $\langle E_k\rangle = \frac{3}{2}Nk_B\theta$. Following Verlet,[5] the contribution to the second term on the right-hand side by the i-th and j-th molecules at a distance over the cutoff length ($|\boldsymbol{x}_i - \boldsymbol{x}_j| > r_{\rm cut}$) can be approximated using the radial distribution function $g(r)$, and so finally we obtain

$$p_{\rm ar} \approx \frac{N}{V}k_B\theta + \frac{1}{6V}\sum_{\substack{j\neq i \\ |\boldsymbol{x}_i - \boldsymbol{x}_j| \leq r_{\rm cut}}}\langle(\boldsymbol{x}_i - \boldsymbol{x}_j)\cdot\boldsymbol{f}(\boldsymbol{x}_j - \boldsymbol{x}_i)\rangle + \frac{N^2}{6V^2}\int_{r_{\rm cut}}^{\infty}\int_0^{\pi}\int_{-\pi}^{\pi} g(r) r \boldsymbol{f}(\boldsymbol{r})\cdot{\rm d}\boldsymbol{r}.$$

Henceforth, we label the sum of the first and second terms on the right-hand side of the above equation by p, and the third term by p'. Table I details the configurations and parameter values of the simulations presented in the present study. In the first two test problems considered in this study, *pc1* and *pc2* in Table I, all the molecules are restricted in a cubic reservoir of dimensions L_x, L_y and L_z, which denote lengths in the x, y, and z directions respectively of the Cartesian coordinate system (x, y, z), with periodic boundary conditions imposed on all the boundary surfaces. For these two systems, p is 0.98, while p' is -0.70 by approximating $g(r) = 1$ for $r > r_{\rm cut}$, hence $p_{\rm ar}$ is approximately 0.28. With reference to the phase diagram shown in Fig. 1, these two systems thus correspond to the liquid phase of argon. This pressure value is smaller than the corresponding values calculated on the basis of the equation of state for the Lennard-Jones molecular fluid realized by Johnson et al[7] ($p_{\rm ar} = 0.303$) and recently by Boltachev et al[8] ($p_{\rm ar} = 0.317$). This difference is largely attributable to the present approximation to $g(r)$, but is also due to the present values of N and $r_{\rm cut}$ being smaller than the values used in these other studies. We additionally confirm that our system

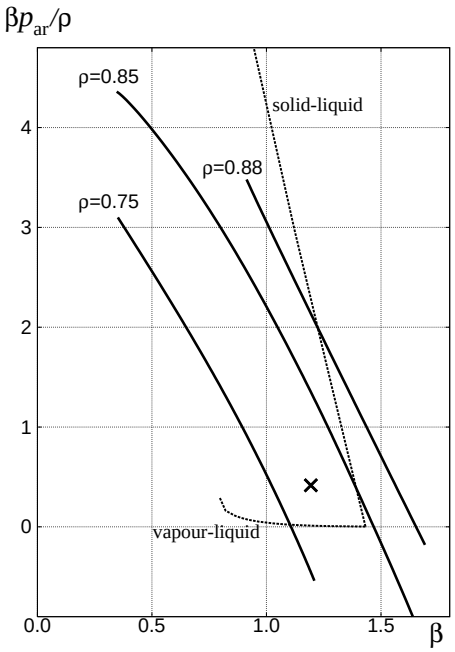

Fig. 1. The compressibility factor $\beta p_{\rm ar}/\rho$ as a function of $\beta = 1/k_B\theta$. The plotted curves correspond to isochores $\rho = 0.88, 0.85, 0.75$ obtained from the MD calculation by Verlet.[5] The values of the compressibility factor for the first two studies in this paper, *pc1* and *pc2* in Table I, are indicated by the cross. The dashed curves correspond to vapour-liquid and solid-liquid coexistence states, found in the experimental study of Din.[9]

is in the liquid state by reference to the θ-ρ projection of phase diagram for a Lennard-Jones molecular fluid.[10]

The pressure calculation based on the virial theorem demonstrated above is generally considered to be applicable to fluid in a reservoir with periodic boundaries; that is an open system without realistic walls. However, the theorem was derived on the assumption that the walls of the reservoir are rigid, reflecting molecules in collision with it, and being thus responsible for imposing the experimentally measurable external pressure. It is therefore more appropriate to simulate a rigid-walled reservoir, so that we can measure the pressure following the original derivation in the theorem. Accordingly, the subsequent studies, *rc1* and *rc2* in Table I, consider a Lennard-Jones molecular fluid in a cubic reservoir enclosed by six square, rigid walls, at which all molecules are reflected in perfectly elastic collisions. The collision of molecules with hard-walls is simulated by applying the velocity Verlet method with a procedure given by the following steps: (1) $\Delta t'$ is set to be Δt, (2) the distribution of molecules are developed up to the minimum collision time t' occurring within $\Delta t'$, which is predicted by solving quadratic equations for the collisions of all the molecules, based on the velocity obtained from the time-development scheme, (3) the normal component of velocity of a molecule in collision with a wall is reversed and $\Delta t'$ is reset to be $\Delta t' - t'$, (4) the above two steps are re-examined

until $\Delta t' = 0$, (5) return to (1). The relative error in energy that arises due to the use of the velocity Verlet method, is confirmed to be less than 0.01 % for the longest time scale performed, $T \sim 10^5$.

The normal stresses (i.e. diagonal components of the stress tensor) for the fluids of these two systems were measured by calculating the impulse of molecules against the examined walls of the reservoir. For example,

$$[\mathcal{P}]_{xx} = \frac{1}{L_y L_z} \langle \int_{L_y L_z} \mathrm{d}\boldsymbol{s} \cdot \boldsymbol{f}(t) \rangle,$$

where $\mathrm{d}\boldsymbol{s} = \mathbf{n} ds$, in which $\mathrm{d}s$ is an infinitesimal area on a wall surface with $\mathbf{n}$ denoting a unit outward-pointing normal to the surface at this point, and $\boldsymbol{f}(t)$ is the force acting on the reflected molecules by this area of the wall. According to Pascal's principle, the three normal stresses in a classical liquid in a static state are all expected to take the value $-p$ due to isotropy. With reference to Table I, it can be seen that the normal stresses for cases *rc1* and *rc2* are in accordance with this principle. This implies the validity of the measurement of the pressure based on computing the impulse of molecules against the walls. Furthermore, it can also be seen from the table that the systems are not significantly affected by changing the boundary conditions from periodic to reflective conditions (cf. *pc1* with *rc1* and *pc2* with *rc2*).

3.2 Liquid in a rectangular-parallelepiped reservoir

We next consider two configurations, *rr1* and *rr2*, which both use domains given by rectangular-parallelepiped reservoirs of size $L_x = 2L_y = 2L_z$. For both these configurations, the reservoirs are again filled with Lennard-Jones molecules, of the same density as that for the cubic reservoirs of the previous configurations. Table I displays the values of p and $[\mathcal{P}]_{ii}$ for these configurations, again measured on the basis of the virial theorem and the measurement of impulse on the wall. It should be noticed that for these two configurations, while $[\mathcal{P}]_{yy}$ and $[\mathcal{P}]_{zz}$ are similar in value, the value of $[\mathcal{P}]_{xx}$ differs from that of the other two normal stresses. This suggests that these two systems may be anisotropic despite the fact that they are static at the macroscopic level. Since anisotropy of the stress tensor under a static state is common in solid phases, but is not common in liquid or gas phases, one may perhaps be tempted to conclude that our molecular fluids are partly crystallized. However, investigating the trajectories of the molecules in these systems, we confirmed that none of the molecules are trapped in tiny regions of the reservoir for a long time.

It may be further noted that for test problems *rr1* and *rr2* the values of the normal stresses (see Table I) all deviate from the negative of the pressure p obtained from the virial theorem . However, this does not constitute a contradiction between the calculations based on the impulse and the theorem. If we relax the assumption of isotropy of the stress tensor in the

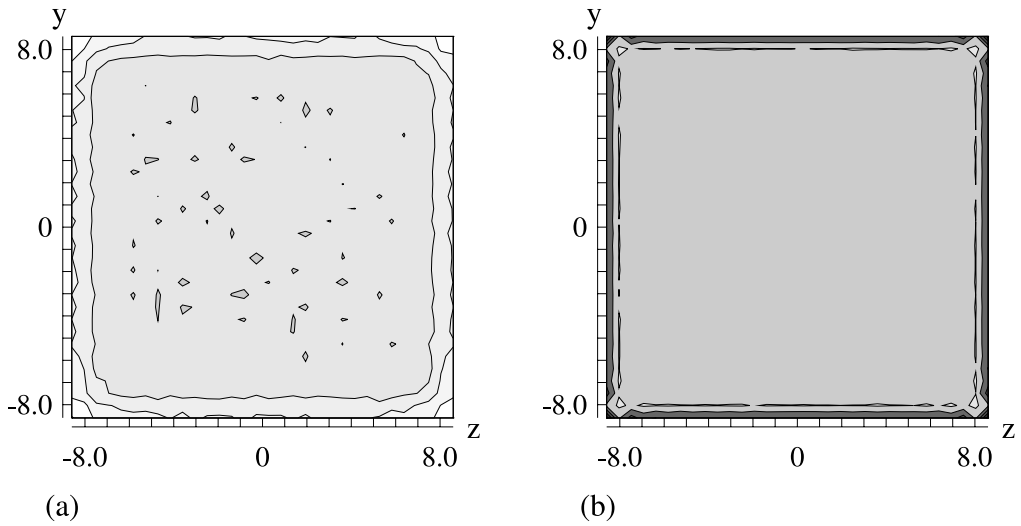

Fig. 2. (a) Contour plot of the ratio of the local density to the mean density is calculated in a thin layer of thickness $\Delta x \approx 0.5$ at the $x = -8.59$ wall of a cubic reservoir with reflective boundaries (*rc2*). The contour levels are $0.6, 0.8, 1.0$ and 1.2. The density is relatively low near the edges, especially near the vertices, but is otherwise comparable with the mean density. (b) Same as (a) but for the case of an alternative Lennard-Jones fluid with $r_{\rm cut} = \sqrt[6]{2}\sigma$ (hard-core potential). The contour levels are 1.2, 2.0, 3.0 and 4.0 . The density is high near the edges and vertices of the reservoir.

derivation of pressure in the virial theorem, we obtain the following relation:

$$p = -\frac{1}{3}\Big([\mathcal{P}]_{xx} + [\mathcal{P}]_{yy} + [\mathcal{P}]_{zz}\Big),$$

which is satisfied for cases *rr1* and *rr2*.

The difference between the value of $[\mathcal{P}]_{xx}$ and that of the other two normal stresses probably results from the size effect of the reservoir, because the difference is larger in *rr1* than in *rr2*. Roughly speaking, pressure depends on density. Thus, the local density of molecules is anticipated to be non-uniform near the walls, which could be prominent in these nanoscale reservoirs. As will be discussed in the next paragraph, this may account for the anisotropy of the normal stress. Indeed, we found that the local density of molecules is relatively low around the edges and vertices of the reservoirs. It is also interesting to note that this phenomenon occurs even in the cubic reservoirs with reflective boundaries, *rc1* and *rc2*. As an example, the local density in a thin layer near a wall of cubic reservoir in *rc2* is shown in Fig. 2(a). This figure suggests that the overall shape of the bulk fluid in *rr1* and *rr2* is a rectangular-parallelepiped with rounded edges and vertices.

Given the low density of molecules in a layer adjacent to the walls of the rigid-walled reservoir, it is of interest to consider the effective volume for a liquid confined in such a reservoir (where the effective volume for a liquid confined in a reservoir with periodic boundary conditions at the walls is of course V). A simple measure can be derived if we simply assume

that there are no molecular collisions within a distance $r_{\rm edge}$ of the walls of the reservoir (i.e. that the liquid occupies an effective volume $V_{eff} = L_xL_yL_z - 4r_{\rm edge}^2(L_x+L_y+L_z) + O(r_{\rm edge}^3) < V$ of rectangular parallelepiped shape), and further assume that the effective pressure is the same at any rectangular wall. Equating the effective pressures at walls $x = L_x/2$ and $y = L_y/2$, we thus have

$$\frac{P_{xx}L_yL_z}{(L_y - 2r_{\rm edge})(L_z - 2r_{\rm edge})} = \frac{P_{yy}L_xL_z}{(L_x - 2r_{\rm edge})(L_z - 2r_{\rm edge})},$$

and so $r_{\rm edge}$ is estimated as 0.63 and 0.58 for *rr1* and *rr2* respectively. These values are fairly smaller than the reservoir scale. As our molecular fluid occupies most of the overall reservoir except for the relatively tiny volume around the edges and vertices, the evaluation of stress based on the impulse on the walls measured within a finite time is supposed to be justified.

To understand the reason for the decrease in local density at the edges and vertices of the reservoir, we performed an extra simulation with the short cutoff length $r_{\rm cut} = \sqrt[6]{2}\sigma$ (hard-core potential) in *rc2*, in which molecules interact only by the repulsive part of the Lennard-Jones potential. At the equilibrium state of this simulation (Fig. 2(b)), the local density at the edges and vertices of the reservoir is relatively higher than the mean density, in contrast to the case with $r_{\rm cut} = 2.5\sigma$. This comparison suggests that the reduction of local density at the edges and vertices is likely to be accounted for by the surface tension yielded by the long-range attractive interaction among the molecules.

3.3 Solutions separated by a semipermeable membrane

Using the molecular liquid described above, in the remainder of this letter we will construct a model of ideal osmotic equilibrium. For osmotic equilibriums in more realistic configurations, the reader is referred to refs. 3,11 and 4. Here, we focus rather on the ideal osmotic equilibrium under a purely idealized situation. As illustrated in Fig.3, the configuration of system *rr2* allows us to obtain a numerical solution for an equilibrium state of ideal solution in contact with a pure solvent across an idealized semi-permeable membrane. This system consists of $N = 8192$ Lennard-Jones molecules, n_1 of which are solute molecules with the remainder ($n_0 = N - n_1$) being solvent molecules. Here, the suffices $i = 0, 1$ refer to the molecule species, solvent and solute, respectively. Consider a semi-permeable membrane of infinitesimal thickness located at $x = 0$, dividing the reservoir into two equal-sized regions A and B as shown in the figure. The initial state is obtained by randomly choosing n_1 solvent molecules in region A to be solute molecules at the aforementioned equilibrium state (attained from simulations performed in *rr2* with neither the solute nor the membrane present). Note that the only difference between solute and solvent molecules in the system is given by the effect of the membrane on these molecules' motions: As well as being confined by the reservoir's walls, the solute molecules are also confined in the region A ($x < 0$), engaging in perfectly elastic collisions with the membrane at $x = 0$. In contrast, the membrane has no effect on the motion

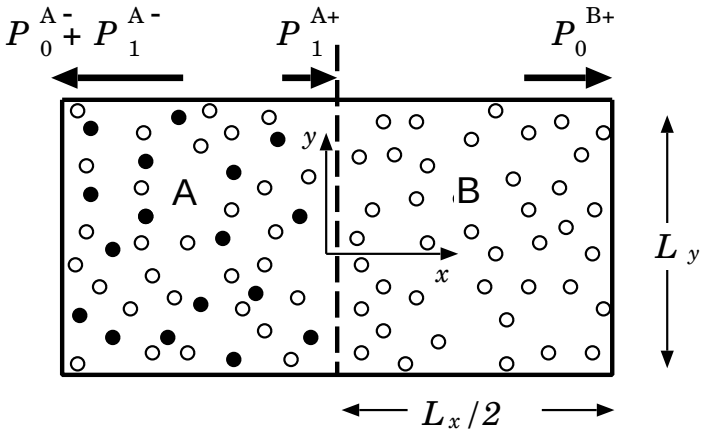

Fig. 3. A schematic view of the $x-y$ projection of the reservoirs (*rr1* and *rr2*). A semi-permeable membrane at $x = 0$ (the thick-dashed line) separates the reservoir into two regions, A and B. The n_0 solvent molecules are represented by open circles ($\circ$), while the n_1 solute molecules are represented by close circles ($\bullet$). The membrane prevents the solute molecules from leaking out of region A, and so the liquids found in regions A and B are a solution and pure solvent, respectively. The thick arrows describe the pressure forces acting on the boundary surfaces and membrane in the x-direction.

of the solvent molecules, with these molecules confined only by the reservoir walls. Thus, for $n_1 > 0$, region A ($x < 0$) contains solution, whereas region B ($x > 0$) contains only pure solvent. It should be noted that the solution can be considered as an ideal solution, because the forces of interaction between solvent and solute molecules are identical to those acting between the solvent molecules themselves. We carried out simulations for $n_1 = 25, 50, 100, 200, 400$ and 800. For simplicity, if we suppose the mean number of molecules in the region A is $N/2$, the range of the concentration of the solution considered here corresponds to $0.006 \sim 0.2$ in mole fractions (0.21 M $\sim$ 6.6 M) .

Denoting the number of the molecules in regions A and B at time t as $n^{\mathrm{A}}(t)$ and $n^{\mathrm{B}}(t)$, respectively, one should examine the long-time average of the excess of n^{X} (X=A,B) over $N/2 = 4096$, which is referred to as $\langle \Delta n^{\mathrm{X}} \rangle$ in what follows. Figure 4 shows the dependence of $\langle \Delta n^{\mathrm{A}} \rangle$ on the concentration n_1/V_A. For the case of no solute we have $\langle \Delta n^{\mathrm{A}} \rangle = \langle \Delta n^{\mathrm{B}} \rangle = 0$, owing to the symmetry of the system. With increasing n_1, $\langle n^{\mathrm{A}} \rangle$ increases (and $\langle n^{\mathrm{B}} \rangle$ decreases) linearly, but with a slope an order of magnitude smaller than that expected for the dilute case, as shown in the figure. Note that if the interactions between molecules were negligible, as in a dilute gas, then $\langle \Delta n^{\mathrm{A}} \rangle = n_1/2$ would be satisfied exactly. In addition, taking into account that an equilibrium state attained with no solute is adopted as the initial distribution for the molecules, we may consider $\langle \Delta n^{\mathrm{A}} \rangle$ as the net number of the solvent molecules that dynamically pass through the membrane in the evolution from the initial equilibrium state.

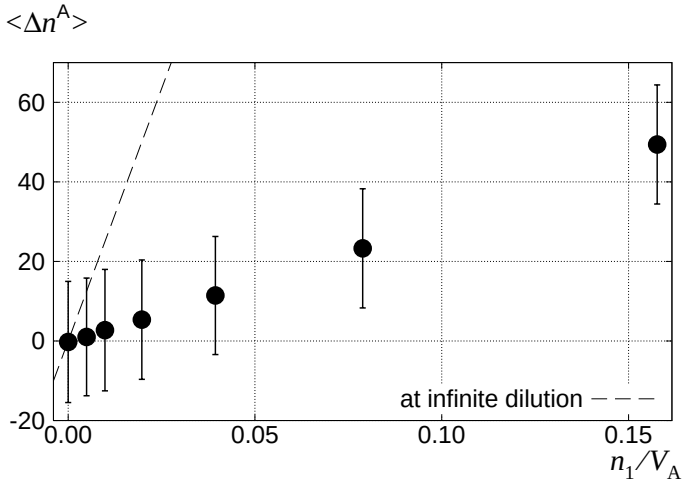

Fig. 4. The dependence of $\langle \Delta n^{\mathrm{A}} \rangle$, the long-time average of the excess of $n^{\mathrm{A}}(t)$ over $N/2(= 4096)$, on the concentration n_1/V_A.

Thus, the increase of $\langle \Delta n^{\mathrm{A}} \rangle$ with n_1 means that dissolving solutes in the solution results in osmotic flow.

Next, let us discuss the osmotic pressure in the systems. We can here consider four kinds of pressures derived from the calculation of impulses: $P_0^{\mathrm{A}-}$ and $P_1^{\mathrm{A}-}$ are the partial pressures on the wall of the reservoir at $x = -L_x/2$ effected by the solvent and solute molecules, respectively, $P_0^{\mathrm{B}+}$ is the pressure on the wall of the reservoir at $x = +L_x/2$ effected by solvent molecules and $P_1^{\mathrm{A}+}$ is the pressure on the membrane at $x = 0$ effected by solute molecules. We assume that the membrane is fixed to the reservoir in such a way so as to maintain its position at $x = 0$ against pressure $P_1^{\mathrm{A}+}$. The long-time average of the net force on the reservoir should vanish, from which we obtain the momentum conservation equation

$$P_0^{\mathrm{A}-} + P_1^{\mathrm{A}-} = P_1^{\mathrm{A}+} + P_0^{\mathrm{B}+}.$$

Because the osmotic pressure is originally defined as the excess pressure of the region A over B that is necessary to prevent a net movement of solvent across the membrane, for the present system the osmotic pressure is given by $(P_0^{\mathrm{A}-} + P_1^{\mathrm{A}-}) - P_0^{\mathrm{B}-}$, that is, $P_1^{\mathrm{A}+}$. The osmotic pressure $P_1^{\mathrm{A}+}$ is shown plotted for different concentrations n_1/V_A by the circles in Fig. 5. Clearly the osmotic pressures found by the present simulations are in excellent agreement with van't Hoff's law for values of n_1/V_A up to 0.04; the law thus appears to be valid over a wide range of concentrations.

4. Discussion

In Fig. 5, we show the partial pressure effected by the solute at $x = -L_x/2$, $P_1^{\mathrm{A}-}$ (the crosses in the figure). Clearly $P_1^{\mathrm{A}-}$ deviates significantly from $P_1^{\mathrm{A}+}$, even for the relatively dilute cases. Thus it is clear that a spatial non-uniformity of the solute partial pressure exists

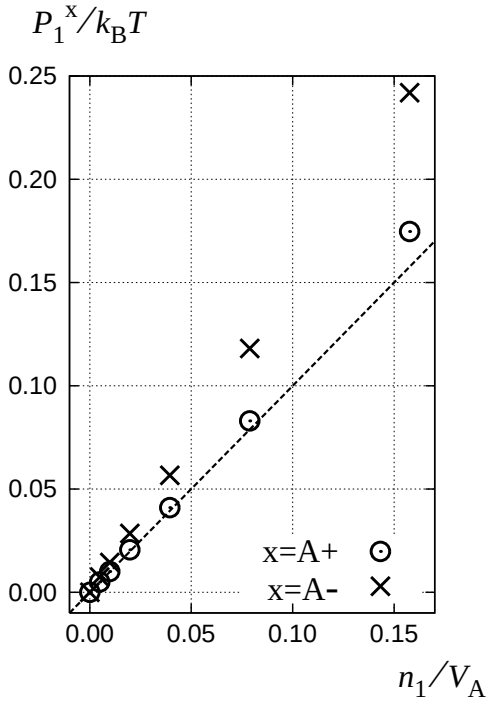

Fig. 5. The dependence of the partial pressures of solute molecules at the membrane, $P_1^{\text{A-}}$ ($\times$), and at the wall of the reservoir at $x = -L_x/2$, $P_1^{\text{A+}}$ ($\circ$), on the concentration n_1/V_A. The dashed line displays values found by van't Hoff's law.

in the solution region of the reservoir, even for the ideal case considered in the present study. Taking the aforementioned equation of momentum conservation into account, we can also deduce from this deviation that $P_0^{\text{A-}} < P_0^{\text{B+}}$. Solvent is, however, kept at rest in the equilibrium state from a macroscopic viewpoint. Therefore, we conclude that the net force exerted by the walls, $L_yL_z(P_0^{\text{B+}} - P_0^{\text{A-}})$, acts on solvent in the negative x direction, and, moreover, that the equivalent force exerted on the solvent by the interaction with the solute molecules is directed in the positive x direction at a macroscopic level.

To understand the spatial distribution of the solute-solvent interaction force and its time development, we introduce $P_{1\to0}(x)$, the local force per unit volume exerted on the solvent by the solute in the positive x direction, which is defined below by summing over all solute-solvent interactions. Referring to the work by Raghunathan and Aluru,[4] we here adopt

$$P_{1\to0}(x)\Delta x L_y L_z = \sum_{i,j}{}' \boldsymbol{f}_{j\to i}\cdot\boldsymbol{e}_x \ ,$$

where $\boldsymbol{e}_x$ is the unit vector in the x direction, the summation over j is taken over all the n_1 solute molecules while that over i is over all the solvent molecules located between x and

$x + \Delta x$. Furthermore, we also introduce the effective potential for solvent $U_{1\to0}(x)$ as

$$U_{1\to0}(x) = -\int_x^{L_x/2} P_{1\to0}(x)\mathrm{d}x \quad .$$

It should be noted that the dimension of $U_{1\to0}(x)$ is that of "stress" in mechanics, but this potential is not a stress in a strict sense, because it relates to the interaction between different types of matter simultaneously occupying the same region of space. Note that $(U_{1\to0}(x) - U_{1\to0}(L_x/2))L_yL_z$ corresponds to the force exerted on the solvent by the solute between x and $L_x/2$. Therefore, $\Delta U L_y L_z$ represents the total interaction force exerted on the entire solvent by the entire solute, where $\Delta U = U_{1\to0}(-L_x/2) - U_{1\to0}(L_x/2)$. Additionally, we have that $\Delta U = P_1^{A-} - P_1^{A+} = P_0^{B+} - P_0^{A-}$ at the equilibrium state. Figure 6 shows $P_{1\to0}(x)$ taken at the initial state (a), at an intermediate time (b), and at the osmotic equilibrium state (c), for the case $n_1 = 800$.

In the equilibrium state (see Fig. 6(c)), some oscillation in $P_{1\to0}(x)$ at the left end of reservoir is clearly observed, which is due to a surface effect caused by the reflective wall located at $x \approx -L_x/2$. This is because the molecules tend to exist only at discrete positions near the wall, $x \approx -L_x/2, -L_x/2 + d, -L_x/2 + 2d, \cdots$, where $d = \sqrt[6]{2}$. This is confirmed by reference to the spatial distribution of local density, which exhibits peaks at these positions. In a more realistic situation, the wall would consist of atoms tethered somehow to lattice sites, so that the peaks would be less distinct. This surface effect is restricted to a layer in a neighbourhood of the wall, approximately described by $x < -12$ for the present configuration, and so it does not significantly affect the results for osmotic flow and pressure, which are the quantities of particular interest to the present study.

For $-12 \le x \le -2$, $U_{1\to0}(x)$ exhibits a plateau-like profile, which implies that the net force exerted on the solvent by the solute is negligible across this relatively wide zone of region A. On the other hand, as can be seen in Fig. 6(c), within a narrow region $(-2 < x < 2)$ about the membrane, $P_{1\to0}(x)$ exhibits an inverted M-shaped profile, while across this region, with increasing x, the value of $U_{1\to0}(x)$ first rapidly increases, then decreases before increasing again to zero. Thus the bulk of the total interaction force, ΔU, that the solute exerts on the solvent is accounted for by this narrow region, with this force exerted in the positive x direction.

This localization of the solute-solvent interaction can be understood intuitively as follows (see Fig. 7). In the equilibrium state, there is an abrupt change in the local density of the solute (and, to a lesser extent, the local density of the solvent) across the membrane. Solvent within a small layer $[x, x+\Delta x]$ inside region A is squeezed equally from both sides of the layer, x and $x + \Delta x$, by the solute molecules distributed uniformly around the solvent. By contrast, close to the membrane, while solvent molecules are pushed in the positive x direction by the solute molecules in region A via the interaction force, there is no counteracting force applied

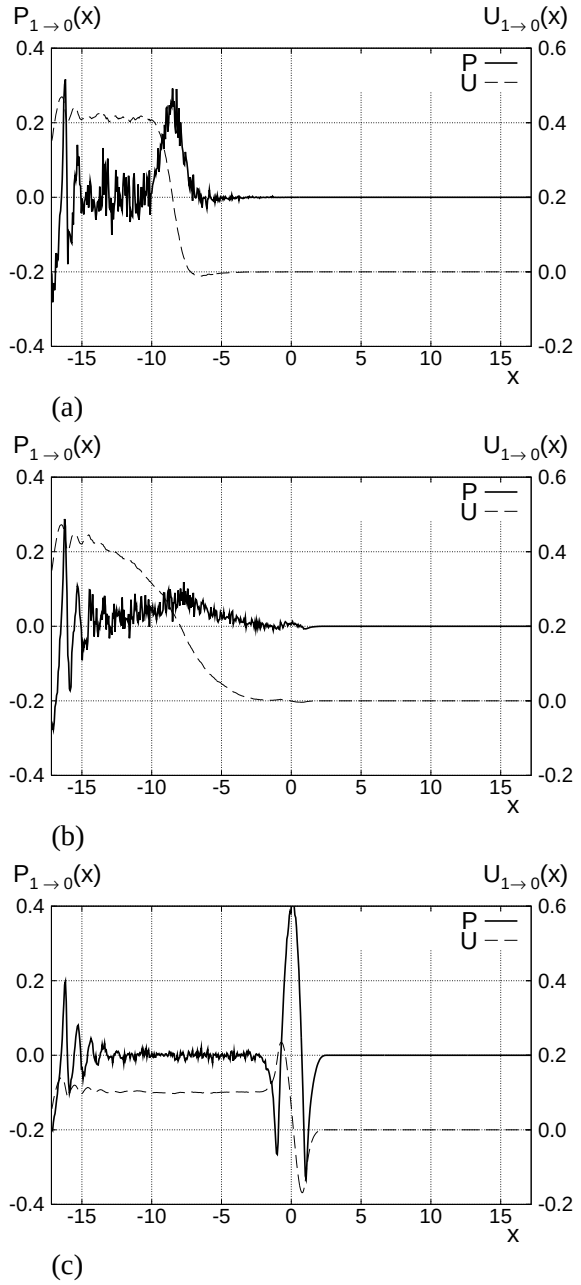

Fig. 6. For $n_1 = 800$, the x component of the local force per unit volume exerted on the solvent by the solute, $P_{1\to0}(x)$, and the effective potential for the solvent due to solute-solvent interaction, $U_{1\to0}(x)$. (a) At $t = 0$,(b) at $t = 100$ and (c) at the osmotic equilibrium state $t > 40000$. The initial state (a) is obtained from the average of more than 60 MD simulations of a pure solvent using different initial conditions.

from region B in the negative x direction, due to the absence of solute in region B. Thus there is a net force in the positive x direction applied to solvent molecules around the membrane, and this results in the localization of the solute-solvent interaction in a neighbourhood of the membrane described above. The repulsive part of the Lennard-Jones potential plays an

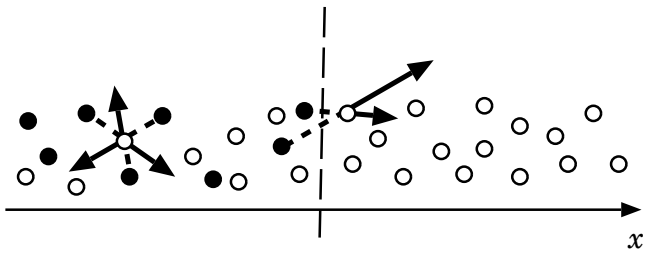

Fig. 7. The force exerted on solvent molecules (○) by solute molecules (●) in region A (left) and across the membrane (shown by the central dashed line), in the equilibrium state.

essential role in this localization, while the effect of the attractive part is also reflected in the couple of small kinks of the $P_{1\to0}(x)$ profile, as seen around $x \approx \pm\sqrt[6]{2}$ in Fig. 6(c) .

We next consider the time-development of the solute-solvent interaction. The initial solute-solvent interaction is larger than that at the equilibrium state. Figure 6(a) shows the statistical average of $P_{1\to0}(x)$ and $U_{1\to0}(x)$ for the initial conditions (where 800 solvent molecules in the region $-L_x/2 < x < -L_x/4$ are randomly selected to be solute molecules from an initial molecular distribution that is the statistical average of many equilibrium states obtained from solvent-only simulations). In the initial state, the profile of $P_{1\to0}(x)$ exhibits similar oscillations in a neighbourhood of the wall at $x = -L_x/2$ as are observed for the equilibrium state in Fig. 6(c) . This phenomenon can again be explained in terms of the surface effect that is present for the equilibrium state attained with no solute present, and does not significantly affect the quantities of particular interest in the present study. We do note, however, the Λ shape of the $P_{1\to0}(x)$ profile in the region $-10 < x < -7$. This region accounts for the bulk of the solute-solvent interaction, $\Delta U \approx 0.4$, which is almost 4 times larger than that of the equilibrium state.

Given some simple assumptions, it can be demonstrated that ΔU is, moreover, a conserved quantity with time in a statistical sense in the early stages of the diffusion. Figure 6(b) shows $P_{1\to0}(x)$ and $U_{1\to0}(x)$ taken at $t = 100$, when there are still relatively few solute molecules near the membrane. From the figure, we can observe that, while solute molecules diffuse in region A and approach the membrane with increasing time, P_1^{A+} and ΔU are approximately maintained at the values 0 and 0.4, respectively, while the Λ-shaped section of the $P_{1\to0}(x)$ profile continues to spread out until the first solute molecule touches the membrane.

Once this Λ-shaped profile has reached the membrane, and sufficient solute molecules become distributed in a neighbourhood of the membrane, ΔU gradually decreases with increasing time, and asymptotically approaches 0.1 in the equilibrium state. The decrease of ΔU is qualitatively accounted for by the "increase of support of the solvent by the membrane" in solute-solvent interaction. That is, by interrupting the diffusion of the solute from region A to B, the membrane begins to support the solvent molecules around the membrane in region

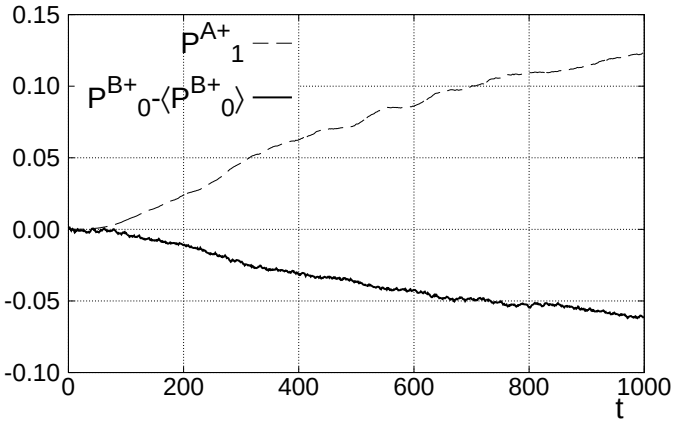

Fig. 8. The time developments of the osmotic pressure P_1^{A+}, and the difference of the pressure in region B compared to the initial pressure in region B obtained from the solvent-only molecular simulations, $P_0^{B+} - \langle P_0^{B+} \rangle$. The value obtained for $\langle P_0^{B+} \rangle$ is obtained from more 60 MD solvent-only simulations employing different initial conditions.

B to exert a force on the solute in region A in the negative x direction. This simultaneously brings about a decrease of the pressure of the solvent in region B. As a consequence, some of the solvent in region B spreads out into region A, which constitutes the osmotic flow in the present study. This is also why P_0^{A-} becomes larger than P_0^{B+} at the equilibrium state. Figure 8 plots the time development of "instantaneous" osmotic pressure, P_1^{A+}, and "instantaneous" pressure in region B, P_0^{B+}, where we have extended the present definitions of pressure (originally defined in terms of the equilibrium state) to be a function of time by introducing ensemble averages taken from many MD simulations. The increase of the osmotic pressure begins with the decrease of pressure in region B. Note that these pressures first start to change from their initial values around $t \approx 80$, the time at which the first solute molecules reach the membrane.

Although it may perhaps seem to be paradoxical from a fluid dynamics point of view that solvent oozes through the membrane from the lower to higher pressure region, the osmotic flow must be caused as a necessary consequence of the "increase of support of the solvent by the membrane", even for the ideal solution realized in the present study.

5. Summary

In summary, an ideal of osmotic equilibrium has been investigated using molecular dynamics. The osmotic flow has been numerically observed as the inflow of the solvent across a membrane from the dilute to the concentrated side. By considering the balance between the partial pressure of solute and solvents, it has been confirmed that van't Hoff's law is valid over a relatively wide range of solute concentrations, and that the partial pressure of the solute

is not uniform in the solution side. Based on the understanding of the non-uniformity of the partial pressure, the mechanism of osmotic flow in the relaxation process as it approaches the equilibrium state has been elaborated on, focusing in particular on the interaction between solute and solvent.

The primary focus of the present study is not to realize a liquid with the precisely-measurable thermodynamical properties at the macroscopic level, but rather to understand the mechanism of solvent transport in a nanofluidic reservoir from the dynamical point of view. To accomplish this aim, it is sufficient to construct a model using a relatively small number of molecules, and to apply a small cutoff length. Future areas of work include the extension of the present model to derive macroscopic results for more realistic, practical fluids.

Acknowledgments

This work has been supported in part by Grant-in-Aid for Scientific Research (B) 16360093 and 19360090, and Grant-in-Aid for Young Scientists(B) 19760123. We also acknowledge financial support by the Kansai University Grant-in-Aid for progress of research in graduate course, 2007. The numerical calculations were partially carried out on SX8 at YITP in Kyoto University. The authors would like to express their cordial thanks to Dr D. P. Wall for improving the manuscript through helpful discussions.

References

1) J. H. van't Hoff: Zeitschrift fur physikalische Chemie **1** (1887) 481.
2) O. Sten-Knudsen: *Biological Membranes* (Cambridge University Press, Cambridge, 2002).
3) S. Murad and J. G. Powles: J. Chem. Phys. **99** (1993) 7271.
4) A. V. Raghunathan and N. R. Aluru: Phys. Rev. Lett. **97** (2006) 024501.
5) L. Verlet: Phys. Rev. Lett. **159** (1967) 98.
6) D. C. Rapaport: *The Art of Molecular Dynamics Simulation* (Cambridge University Press, Cambridge, 1995).
7) J. K. Johnson, J.A. Zollweg, and K. E. Gubbins: Molecular Physics **78** (1993) 591.
8) G. S. Boltachev and V. G. Baidakov: High Temperature **41** (2003) 314.
9) F. Din: *Thermodynamic Functions of Gases* (Butterworths Scientific Publications, London, 1956).
10) D. A. Kofke: J. Chem. Phys. **98** (1993) 4149.
11) S. Murad, K. Oder, and J. Lin: Molecular Physics **95** (1998) 401.